High Number of Transport Modes: A Requirement for Contact Resistance Reduction to Atomically Thin Semiconductors

Emanuel Ber, Ryan W. Grady, Eric Pop, *Fellow, IEEE*, and Eilam Yalon

***Abstract*— Electrical contacts to atomically thin 2-D semiconductors are considered as the hindering aspect of electronic devices based on these materials. The high resistance of such contacts stems from their Schottky nature in contrast to the desired low-resistance Ohmic contacts. This issue of Schottky contacts is thus one of the major inhibitors to the integration of 2-D materials into mainstream technology. In this work, we explore contact resistance (R_C) to atomically thin 2-D semiconductors in terms of the injected current through the Schottky barrier (SB) by using the Landauer–Büttiker formalism as well as experimental measurements and technology computer aided design (TCAD) simulations. We show that the SB height and width, which are determined by the metal–semiconductor interface and the number of charge carriers in the semiconductor channel, respectively, affect R_C when it is relatively high ($R_C > 1$ k$\Omega\cdot\mu$m). However, the number of transport modes for carrier injection is the limiting factor for aggressive R_C lowering ($R_C < 1$ k$\Omega\cdot\mu$m), even for near-zero SB height. Our results show that to reduce R_C below 100 $\Omega\cdot\mu$m, large number of transport modes are required, which can be accomplished through raising the number of channel carriers above $5\cdot10^{13}$ cm^{-2} by means of heavy doping or gating. Our conclusions offer insight for future contact engineering and can explain recently published state-of-the-art results.**

***Index Terms*— Contact resistance, field-effect transistor (FET) modeling, Schottky barrier (SB), transport modes.**

I. Introduction

AS ATOMICALLY thin 2-D materials gain more attention due to their outstanding properties and extreme thinness, it becomes apparent that high contact resistance (R_C) is one of their major drawbacks [1], [2], [3]. Much effort has recently been invested to lower R_C to 2-D semiconductors by increasing their charge carrier concentration (n) or by depinning the Fermi level at the metal/semiconductor interface [4], [5], [6], [7], [8], [9], [10], [11], [12]. However, the calculations of the intrinsic lower limit of contact resistivity to bulk semiconductors showed that the number of states available for carrier transport determines R_C at the extreme end of scaling [13], [14]. Therefore, which of these approaches will reduce R_C more dramatically remains an open question. Moreover, the main determining factor of R_C and its relation to the aforementioned methods in the context of atomically thin 2-D semiconductors have not been thoroughly discussed.

Here, we address the questions of preferred method and limiting factor for aggressive R_C reduction by utilizing a combination of three approaches. First, the usage of an analytical Schottky barrier field-effect transistor (SB-FET) model and application of various physics driven modifications. Second, the detailed experimental analysis of R_C and the Schottky barrier (SB) height (ϕ_B) to monolayer (1L) MoS_2. Third, the simulation of R_C with Sentaurus technology computer aided design (TCAD) software [15], [16], [17]. First, we calculated the current injected through an SB between MoS_2 and metal contacts using the Landauer–Büttiker formalism with ϕ_B and n acting as the model parameters [16], [18]. Previously, the model was only used for current calculations in the SB-FET OFF-state, and our adjustments enable its use in the ON-state as well, thus allowing for R_C to be extracted at the desired transistor operation mode. Then, to complement the model modifications, we fabricated 1L MoS_2 transistors with Ni contacts in four-point probe (4PP) measurement structures and compared the experimentally extracted current and contact resistance to the model calculated values [17]. Finally, we validated the results by conducting TCAD simulations of 1L MoS_2 structures and extract R_C by using the SB-FET model parameters as simulation inputs. We see that the SB width and height equivalently affect the current when the contact resistance is relatively high and crucially find that for extreme R_C reduction, the critical limiting factor is the number of transport modes for injection and not the transmission coefficient through the barrier. Our results show that high

Manuscript received 5 December 2022; revised 20 January 2023; accepted 7 February 2023. Date of publication 28 February 2023; date of current version 24 March 2023. This work was supported in part by the Israel Innovation Authority Nofar Program under Grant 78283, and in part by the Russell Berrie Nanotechnology Institute (RBNI). The review of this article was arranged by Editor J. Mateos. *(Corresponding author: Eilam Yalon.)*

Emanuel Ber and Eilam Yalon are with the Viterbi Faculty of Electrical and Computer Engineering, Technion—Israel Institute of Technology, Haifa 32000, Israel (e-mail: semanbar@technion.ac.il; eilamy@technion.ac.il).

Ryan W. Grady and Eric Pop are with the Electrical Engineering Department, Stanford University, Stanford, CA 94305 USA (e-mail: epop@stanford.edu).

Color versions of one or more figures in this article are available at https://doi.org/10.1109/TED.2023.3244512.

Digital Object Identifier 10.1109/TED.2023.3244512

number of transport modes, achievable by increasing n, are needed to reach desirably low R_C even for low ϕ_B, implying that high n is essential in lowering R_C to atomically thin semiconductors.

II. Current Modeling of SB-FET

The calculation of the current and contact resistance using the SB-FET model relies on the Landauer–Büttiker formalism, which accounts for two modes of current injection, namely, thermionic emission over the SB and field emission (tunneling) through the SB [16], [18]. The injected electron current is expressed as

$$I = 2q/h \int_{E_c}^{\infty} M(E)T(E)\big[f(E) - f(E + qV_C)\big]dE \quad (1)$$

where I is the current, q is the electron charge, h is Planck's constant, $M(E)$ is the number of transport modes for conduction in the semiconductor channel, $T(E)$ is the transmission coefficient through the barrier, $f(E)$ is the Fermi-Dirac distribution, and V_C is the voltage drop across the contacts. Note that because our purpose is to understand which aspect of the SB limits the reduction of R_C, we assume that the current is contact-resistance-limited and therefore do not include carrier scattering inside the channel in our current model. Furthermore, we only address the case of long contacts that are not limited by the contact transfer length. However, for aggressively scaled contacts, more considerations should be applied to accommodate the further limiting factor. We choose to model the current as a result of the contact voltage drop, which we experimentally determine and separate later on. The total current is thus the sum of the charge carrier transmission across all the available transport modes for conduction at energies above the conduction band edge for a given V_C.

The above expression is valid when the current is primarily governed by electron injection into the conduction band but can readily be adjusted for hole injection into the valence band. The resulting current for $E < \phi_B$ (i.e., tunneling through the barrier) is dominated by field emission and thermionic field emission, and for $E > \phi_B$, the resulting current is dominated by thermionic emission. We calculate $M(E)$ by counting the number of modes along the transport direction in the first Brillouin zone, as previously shown by Suryavanshi et al. [19]. The subtraction of the Fermi-Dirac distributions ensures that the number of electrons participating in the conduction is determined exclusively by V_C [16].

The transmission coefficient is normally calculated by assuming a fully depleted conducting channel and a triangular-shaped SB with a base width equal to the characteristic geometrical screening length (λ_{geo}) [15], [16], [20]. The length is defined by [21]

$$\lambda_{geo} = \sqrt{(\epsilon_{2D}/\epsilon_i)t_i t_{2D}} \quad (2)$$

where ε_{2D} is the 2-D channel dielectric constant, ε_i is the gate insulator dielectric constant, t_i is the gate insulator thickness, and t_{2D} is the 2-D channel thickness, resulting in a constant λ_{geo} for a given FET. This extraction process is therefore valid for SB-FETs operating in the OFF-state where these assumptions hold. When the SB-FET operates in the ON-state however, high carrier density is induced by the gate inside the channel, and it is therefore no longer fully depleted. To overcome the limitations imposed by the above assumptions, we adjusted the transmission coefficient calculation based on previous work that detail the expansion of the SB into the channel of FETs based on 2-D materials (2-D-FETs) [22], [23].

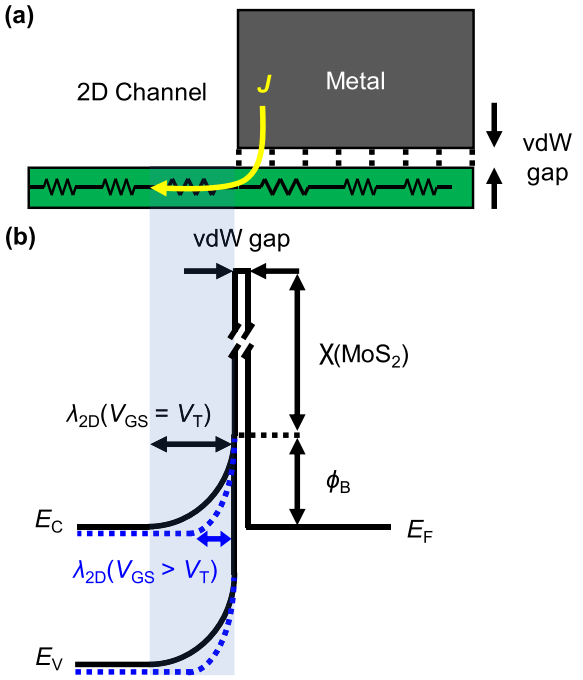

Fig. 1. (a) Schematic of the current path from metal to semiconductor. (b) Corresponding band diagram. The injected carries must tunnel through the vdW gap and the SB. The barrier width (λ_{2D}) strongly depends on the back-gate voltage as shown in blue.

First, we adjust the SB width to accurately reflect the electrostatic effect resulting from the carrier concentration in the channel induced by the back-gate voltage. As discussed previously by Kang et al. [22], the band-bending due to the SB must decay across the 2-D channel when the dielectric screening length is longer than the channel thickness, as shown in Fig. 1. The barrier penetration length inside the 2-D channel (λ_{2D}) is determined by solving Poisson's equation and given by

$$\lambda_{2D} = \sqrt{\frac{2\epsilon_0\epsilon_{2D}\big[\phi_B/q + 0.5V_C + G(V_{GS} - V_T)\big]}{qn}} \quad (3)$$

where ε_0 is the vacuum permittivity, V_{GS} is the back-gate voltage, V_T is the FET threshold voltage, and G is the band movement factor that determines the ratio between the back-gate voltage and the band-bending [24]. The 1-D solution of Poisson's equation is best suited for 1L channels, while thicker multilayered channels may require a more detailed 2-D solution to calculate λ_{2D}, like bulk semiconductors. However, the main point of the manuscript still holds as the limiting factor of R_C will remain as discussed by Baraskar et al. [13] and Maassen et al. [14]. For simplicity, we assume that the applied voltage V_C distributes equally between the source and drain contacts, and therefore, only half of it drops on each one, resulting in the 0.5 coefficient in the above expression.

Note that this is likely not the case due to the inherent different nature of current injecting and collecting contacts and the contact-to-contact variability in a fabricated device [23]. The band movement factor is given by

$$G = \left(1 + \frac{t_i \epsilon_{2D}}{t_{2D} \epsilon_i}\right)^{-1} \tag{4}$$

and is derived from the solution of a series capacitance network [24]. The channel charge carrier concentration during the ON-state operation of the FET (i.e., for $V_{GS} > V_T$) induced by the back-gate voltage is given by

$$n = C_i(V_{GS} - V_T - 0.5V_C)/qt_{2D} \tag{5}$$

where C_i is the back-gate insulator capacitance.

We divide by the 2-D channel thickness to transition between the surface charge concentration and the volume charge concentration. The barrier width is expectedly found to be gate-dependent at these conditions.

Second, we modify the transmission coefficient calculation to consider the entire current path and account for the varying λ_{2D}.

For most contacts to 2-D semiconductors, when charge carriers are injected from the metal into the semiconductor channel, they must pass through a van der Waals (vdW) gap prior to the SB, as shown in Fig. 1(a) [22], [25]. A band diagram representing the energy barriers along the current path is shown in Fig. 1(b), note that λ_{2D} depends on the back-gate voltage, as shown schematically in blue. The transmission of electrons through the vdW gap (T_{vdW}) is calculated using the Wentzel–Kramer–Brillouin (WKB) approximation and is given by the rectangular potential barrier tunneling probability

$$T_{vdW}(E) = \exp\left(-2L_{vdW}\sqrt{8\pi^2 m_e(\chi_{2D} - E)}/h^2\right) \tag{6}$$

where L_{vdW} is the vdW gap width, m_e is the electron effective mass, and χ_{2D} is the 2-D material electron affinity, which acts as the vdW gap height. We used a 3-Å-wide gap for our calculation to coincide with previous work [19] resulting in $T_{vdW} = 1\%$–2%; however, various MoS_2-metal bond lengths have previously been reported [22]. By adjusting for the correct vdW gap width, the model can be generalized for any atomically thin semiconductor–metal contact.

The transmission coefficient through the SB (T_{SB}) is also calculated using the WKB approximation and is then given by

$$T_{SB}(E) = \exp\left(-\frac{8\pi}{3h} \cdot \frac{\sqrt{2m_e(\phi_B - E)^3}\lambda_{2D}}{\phi_B + q[G(V_{GS} - V_T) + 0.5V_C] - E_c}\right). \tag{7}$$

The transmission coefficient through the barriers is therefore

$$T(E) = T_{vdW}(E) \cdot T_{SB}(E) \tag{8}$$

and is used for the current calculation shown in (1). Any spatial variations affecting the carrier injection, such as SB height inhomogeneity [26], [27], can be accounted for by implementing a variance function into the relevant variable [e.g., $\phi_B(x)$] in the transmission coefficient and barrier penetration length calculations.

We conduct further analysis to complement our modeling efforts by experimentally obtaining ϕ_B and n and using them as the key parameters for comparison with our model results. Note that n affects not only λ_{2D} but also the number of transport modes through the change in the conduction band edge location. As n increases, the conduction band edge approaches the 2-D semiconductor Fermi level and becomes lower relative to the metal Fermi level. As presented by Suryavanshi et al. [19], the number of transport modes monotonically increases for energy states above the conduction band edge. Therefore, increasing n allows the metal to inject electrons into relatively higher energy states with respect to the semiconductor conduction band edge, which are associated with larger number of transport modes.

To test our approach experimentally we patterned 4PP test structures by e-beam lithography and used e-gun evaporated Ni as contacts to MoS_2 grown by chemical vapor deposition (CVD) on SiO_2 (90 nm)/Si (p++) substrates, where the Si serves as a back-gate, as illustrated in Fig. 2(a) [28]. As was previously reported, Ni can form chemical reaction free contacts to MoS_2, therefore exhibiting a vdW gap [29], [30], [31]. An atomic force microscopy image of the device structure is presented in Fig. 2(b), and more details on the device fabrication are reported elsewhere [23]. I_D–V_{GS} measurements, presented in Fig. 2(c), show typical gate control with I_{on}/I_{off} ratio $> 10^8$ and 20-μA/μm current at $V_{GS} = 40$ V and $V_{DS} = 1$ V for a 3-μm-long device. The measurements were performed at various temperatures ranging from 125 to 300 K in vacuum ambient condition of $3{\cdot}10^{-5}$ mbar. The subthreshold current increases with the temperature due to the higher contribution of the thermionic current that is suppressed at lower temperatures. Fig. 2(d) and (e) depicts the determination of the SB height by first extracting the slopes of $\ln(I_D/T^{1.5})$ versus $1000/T$ for various gate biases, then choosing the barrier height at flat band conditions from the effective barrier height versus V_{GS} plot as the point at which the relation diverges from linearity [15]. The SB height is found to be $\phi_B \approx 150$ meV.

The calculated and measured current versus charge carrier concentration is presented in Fig. 3(a). The physical parameters used for calculations are $\varepsilon_{2D} = 4$, $\varepsilon_i = 3.9$, $m_e = 0.45m_0$, $\chi_{2D} = 4.05$ eV, and $L_{vdW} = 3$ Å. We used 4PP measurements to determine and separate the effective contact voltage drop ($V_{DS,eff}$) as previously mentioned by subtracting the channel region voltage drop (V_{Ch}) from the applied voltage V_{DS} [17]. V_{Ch} is given by

$$V_{Ch} = V_{2-3}\frac{L_{Ch}}{L_{2-3}} \tag{9}$$

where V_{2-3} is the voltage drop between contacts 2 and 3, L_{Ch} is the total channel length, and L_{2-3} is distance between contacts 2 and 3. The voltage used for the current modeling calculation is then adjusted accordingly. Although the main assumption of our contact resistance model is that the current is contact-resistance-limited, it does not necessarily hold for the fabricated 4PP devices. In fact, the fabricated channels are 3 μm long and the device currents are channel-resistance-limited. However, by accounting for the effective voltage drop on the contacts, we can compare the modeled and

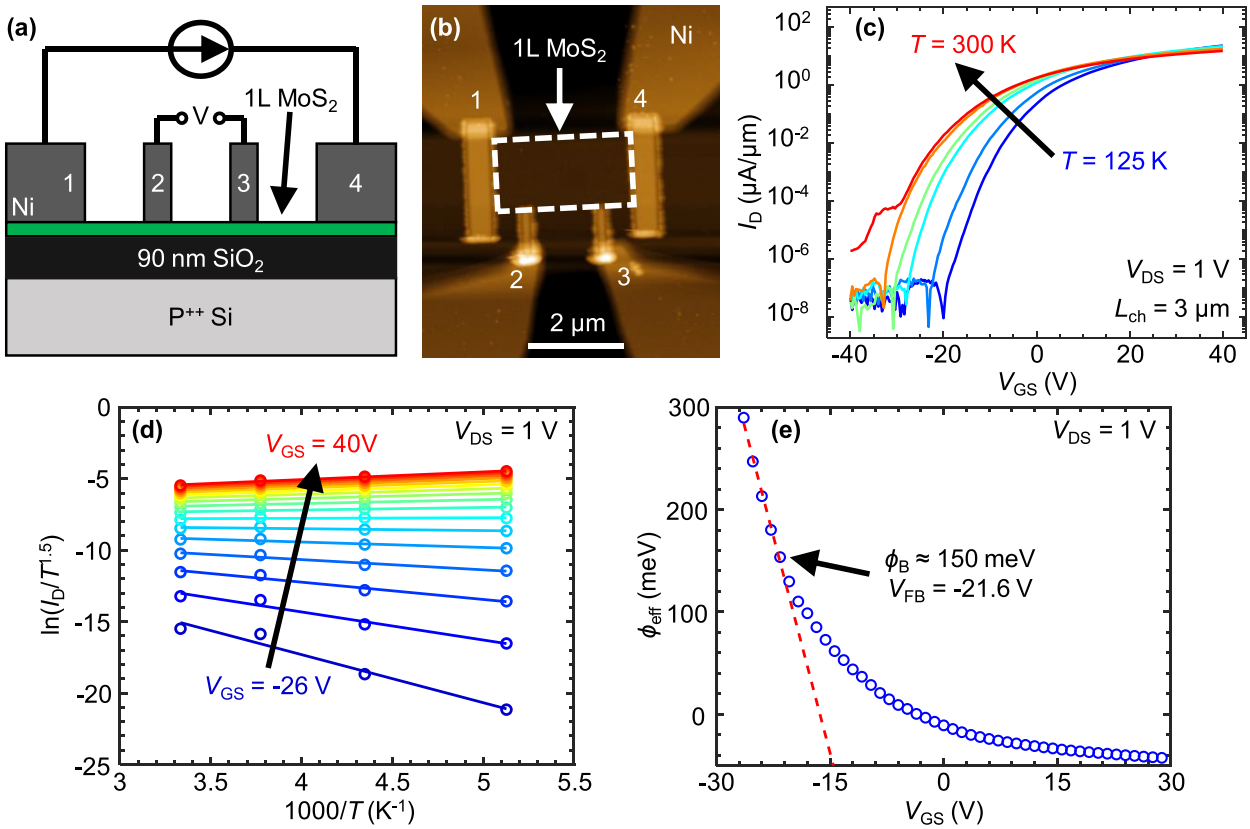

Fig. 2. (a) Schematic of 1L MoS_2 4PP device structure. (b) Atomic force microscopy image of the fabricated device. (c) Corresponding temperature dependent I_D–V_{GS} measurements. The characteristics show typical behavior of $I_D \approx 20$ μA/μm at $V_{GS} = 40$ and $V_{DS} = 1$ V, with $I_{on}/I_{off} > 10^8$. T is varied between 125 and 300 K to extract the SB. (d) $\ln(I_D/T^{1.5})$ versus $1000/T$ for various gate voltages. The markers represent the experimental data, and the lines represent linear regression. (e) Effective barrier height versus gate voltage. The SB height is extracted at flat-band conditions, where the relation deviates from linearity.

experimentally measured currents using the aforementioned effective voltage drop adjustment. The experimentally extracted and modeled R_C versus n is presented in Fig. 3(b), showing the well-known back-gate voltage dependency of R_C [32]. Our modeled I and R_C both exhibit good agreement with the measurements, affirming the model modifications we made. Some mismatch is observed which can be attributed to our assumptions that the voltage drop distributes equally between the source and drain contacts and to the process variability of the MoS_2 growth and contact metal deposition.

Lastly, we compare our modeled R_C with values obtained from Sentaurus TCAD simulations and evaluate the relative effect of the SB height and width on R_C using both methods. The barrier height is adjusted with the variation of ϕ_B, and the barrier width is adjusted with the variation of n (and λ by consequence). Besides varying n, we account for the V_{GS} effect on R_C by inserting the band bending induced by the back-gate voltage into the transmission coefficient calculation. The structure used for the TCAD simulations is similar to previous publications [33], [34], [35]. Briefly, a single layer of MoS_2 with 0.6 nm thickness is defined on top of a SiO_2/Si substrate to reflect the fabricated 1L MoS_2 devices. A 3-Å-wide vdW gap between the MoS_2 layer and the metal contacts is modeled by a vacuum layer ($\varepsilon = 1$) in the designated area. The simulation then solves Poisson's equation coupled with drift-diffusion equations, and the boundary conditions we set act as the applied gate and drain voltages.

First, we can examine the similarity between our modified model and the TCAD simulation by comparing the band structure used for the R_C calculation. Fig. 4(a) and (b) shows Poisson's equation and the intricate numerical solutions for the band structure, respectively, for a 150-meV SB. The lateral decay of the bands is clearly shown by the large scale for the x-axis in comparison to the 1L thickness. The numerical solution provided by TCAD simulations is more exact but requires high computation power to achieve, and the simple Poisson's equation solution however is less accurate but is considerably easier to obtain. Therefore, we can use our calculation for the barrier penetration length, λ_{2D}, as a good estimate.

Fig. 4(c) and (d) displays the calculated heat maps of R_C as a function of ϕ_B and n as extracted from our model and TCAD simulations, respectively. The markers represent reported state-of-the-art experimental data, and the dashed lines represent the 1000-, 500-, and 200-$\Omega\cdot\mu$m contours [4], [6]. The general trends of R_C are similar between our model and the TCAD simulation, again reiterating the power of our model to evaluate R_C with a simple calculation as opposed to a robust numerical differential equation solver. We note that although a specific value for the vdW gap width (3 Å) is used for the MoS_2-Ni contact, other values can otherwise be used to account for different atomically thin semiconductor–metal contact interfaces. Fig. 5 shows the model and TCAD simulation calculation of R_C for various vdW gap widths, showing the generalization of both the model and simulation. Note that due to software limitations, the TCAD R_C computation uses

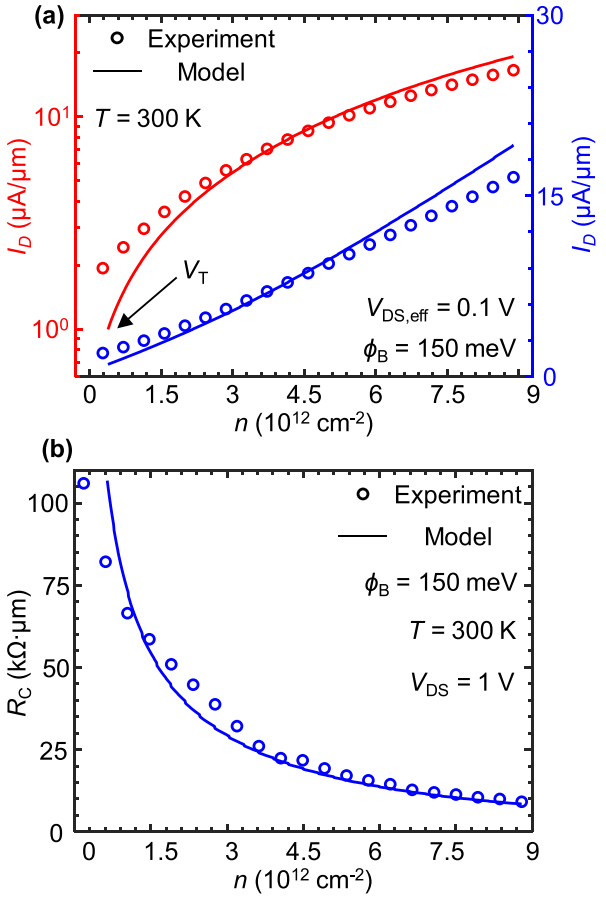

Fig. 3. Comparison between measured and modeled contact characteristics, markers represent the experimental data and the lines represent the model results. (a) Measured and calculated current versus carrier concentration in log (red) and linear (blue) scale. $V_{DS,eff}$ is the experimentally separated voltage drop across the contacts, determined by subtracting the contribution of the channel using the 4PP structure. This extracted value is used for the current modeling to accurately compare the contact characteristics. (b) Experimentally extracted and modeled R_C versus n. All values are plotted for $V_{GS} > V_T$.

parabolic band structure and density of states (DOS), instead of the 1L MoS_2 DOS calculated by Suryavanshi et al. [19]. When calculating the R_C heat map using our model with parabolic bands, mirroring the TCAD simulation, we observe similar trends; however, the absolute values of R_C are marginally larger when parabolic bands are used.

In the midrange of R_C (~1 kΩ·μm), we observe from our model and TCAD results a dependency on both ϕ_B and n as there is no clear factor limiting the current. However, to reach desirably low R_C (<200 Ω·μm), high carrier concentrations (narrow SB and large number of transport modes) are required even for near-zero SB height, suggesting that high n is crucial in reducing R_C to 2-D semiconductors [36]. Interestingly, when n is increased beyond $3{\cdot}10^{13}$ cm^{-2}, the R_C dependency on ϕ_B weakens as the transmission coefficient through the SB becomes close to unity (T_{vdW} is independent on n). This stems from the strong dielectric screening that dramatically reduces the SB width, which greatly increases the tunneling probability and makes the SB height a lesser determining aspect of the transmission coefficient. We thus see that the number of transport modes limits the current at low or near-zero ϕ_B. We note that this could also limit edge contacts,

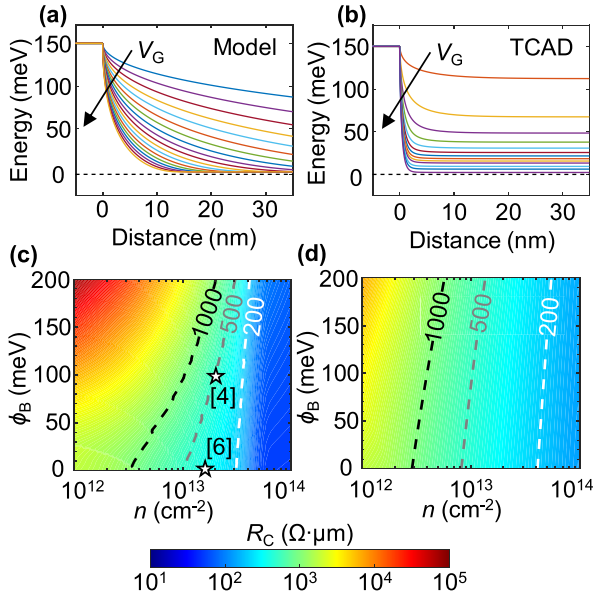

Fig. 4. Calculated band structure from (a) our model and (b) TCAD simulation for a 150-meV SB between the metal contact and 1L MoS_2 channel. Calculated R_C heat maps as a function of ϕ_B and n extracted from (c) our model and (d) TCAD simulation. The carrier concentration axis and contact resistance scale are logarithmic. The markers represent the reported state-of-the-art experimental data, and the dashed lines represent the 1000-, 500-, and 200-Ω·μm contours.

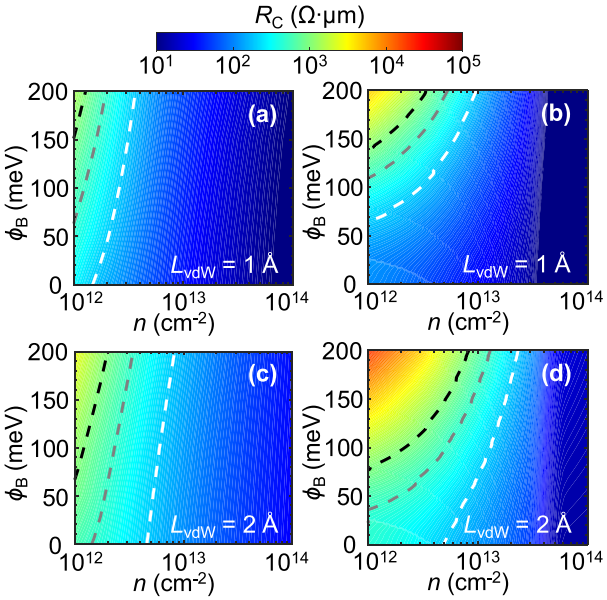

Fig. 5. Calculated R_C heat maps as a function of ϕ_B and n extracted from (a) and (c) TCAD simulation and (b) and (d) our model for various vdW gap widths as labeled in each panel. The dashed lines represent the 1000- (black), 500- (gray), and 200-Ω·μm (white) contours.

which potentially shunt and reduce the vdW gap, as shown in the heat maps presented in Fig. 5 [22].

III. Conclusion

In conclusion, our work shows that although both the SB height and width generally determine R_C, the increase of carrier concentration is more consequential in reducing R_C to 500 Ω·μm and beyond. We found that for such low R_C, the

major current injection limiting factor is the number of transport modes (determined by n), while the transmission coefficient (and by extent ϕ_B) has a lesser effect. Our results suggest that increasing the carrier concentration (e.g., by strong gating or doping) is a prerequisite for aggressively lowering R_C, for example, $n > 5{\cdot}10^{13}$ cm^{-2} is needed to reduce R_C below 100 $\Omega{\cdot}\mu$m even for near-zero ϕ_B [5], [10], [37], [38]. These findings can help explain recent state-of-the-art results and provide a guideline for future contact engineering to atomically thin 2-D semiconductors.

Acknowledgment

Fabrication was carried out at the Technion Micro-Nano Fabrication & Printing Unit (MNF&PU).

References

[1] S. Das et al., "Transistors based on two-dimensional materials for future integrated circuits," *Nat. Electron.*, vol. 4, pp. 784–799, Nov. 2021, doi: 10.1038/s41928-021-00670-1.

[2] D. Akinwande et al., "Graphene and two-dimensional materials for silicon technology," *Nature*, vol. 573, pp. 507–518, Sep. 2019, doi: 10.1038/s41586-019-1573-9.

[3] Z. Cheng, K. Price, and A. D. Franklin, "Contacting and gating 2-D nanomaterials," *IEEE Trans. Electron Devices*, vol. 65, no. 10, pp. 4073–4083, Oct. 2018, doi: 10.1109/TED.2018.2865642.

[4] C. J. McClellan, E. Yalon, K. K. H. Smithe, S. V. Suryavanshi, and E. Pop, "High current density in monolayer MoS_2 doped by AlO_x," *ACS Nano*, vol. 15, no. 1, pp. 1587–1596, Jan. 2021, doi: 10.1021/acsnano.0c09078.

[5] P.-C. Shen et al., "Ultralow contact resistance between semimetal and monolayer semiconductors," *Nature*, vol. 593, no. 7858, pp. 211–217, May 2021, doi: 10.1038/s41586-021-03472-9.

[6] L. Liuet al., "Uniform nucleation and epitaxy of bilayer molybdenum disulfide on sapphire," *Nature*, vol. 605, pp. 69–75, May 2022, doi: 10.1038/s41586-022-04523-5.

[7] Y. Liu et al., "Approaching the Schottky-Mott limit in van der Waals metal-semiconductor junctions," *Nature*, vol. 557, no. 7707, pp. 696–700, May 2018, doi: 10.1038/s41586-018-0129-8.

[8] C.-S. Pang, P. Wu, J. Appenzeller, and Z. Chen, "Thickness-dependent study of High- performance WS_2-FETs with ultrascaled channel lengths," *IEEE Trans. Electron Devices*, vol. 68, no. 4, pp. 2123–2129, Apr. 2021, doi: 10.1109/TED.2021.3058078.

[9] C.-C. Chiang, H.-Y. Lan, C.-S. Pang, J. Appenzeller, and Z. Chen, "Air-stable P-doping in record high-performance monolayer WSe_2 devices," *IEEE Electron Device Lett.*, vol. 43, no. 2, pp. 319–322, Feb. 2022, doi: 10.1109/LED.2021.3135312.

[10] A.-S. Chou et al., "High on-state current in chemical vapor deposited monolayer MoS_2 nFETs with Sn ohmic contacts," *IEEE Electron Device Lett.*, vol. 42, no. 2, pp. 272–275, Feb. 2021, doi: 10.1109/LED.2020.3048371.

[11] A. Rai et al., "Air stable doping and intrinsic mobility enhancement in monolayer molybdenum disulfide by amorphous titanium suboxide encapsulation," *Nano Lett.*, vol. 15, no. 7, pp. 4329–4336, Jul. 2015, doi: 10.1021/acs.nanolett.5b00314.

[12] C. J. Lockhart de la Rosa et al., "Highly efficient and stable MoS_2FETs with reversible n-doping using a dehydrated poly(vinyl-alcohol) coating," *Nanoscale*, vol. 9, no. 1, pp. 258–265, 2017, doi: 10.1039/C6NR06980K.

[13] A. Baraskar, A. C. Gossard, and M. J. W. Rodwell, "Lower limits to metal-semiconductor contact resistance: Theoretical models and experimental data," *J. Appl. Phys.*, vol. 114, no. 15, Oct. 2013, Art. no. 154516, doi: 10.1063/1.4826205.

[14] J. Maassen, C. Jeong, A. Baraskar, M. Rodwell, and M. Lundstrom, "Full band calculations of the intrinsic lower limit of contact resistivity," *Appl. Phys. Lett.*, vol. 102, no. 11, Mar. 2013, Art. no. 111605, doi: 10.1063/1.4798238.

[15] S. Das, H.-Y. Chen, A. V. Penumatcha, and J. Appenzeller, "High performance multilayer MoS_2 transistors with scandium contacts," *Nano Lett.*, vol. 13, no. 1, pp. 100–105, Jan. 2013, doi: 10.1021/NL303583V.

[16] A. V. Penumatcha, R. B. Salazar, and J. Appenzeller, "Analysing black phosphorus transistors using an analytic Schottky barrier MOSFET model," *Nature Commun.*, vol. 6, pp. 8948-1–8948-8, Nov. 2015, doi: 10.1038/ncomms9948.

[17] C. Pang et al., "Mobility extraction in 2D transition metal dichalcogenide devices—Avoiding contact resistance implicated overestimation," *Small*, vol. 17, no. 28, Jul. 2021, Art. no. 2100940, doi: 10.1002/SMLL.202100940.

[18] S. Datta, *Electronic Transport in Mesoscopic Systems*. Cambridge, U.K.: Cambridge Univ. Press, 1997, pp. 42–65.

[19] S. V. Suryavanshi et al., "Improving electric contacts to two-dimensional semiconductors," 2021, *arXiv:2105.10792*.

[20] M. Houssa, A. Dimoulas, and A. Molle, Eds., *2D Materials for Nanoelectronics*. Boca Raton, FL, USA: CRC Press, 2016, pp. 207–239.

[21] R.-H. Yan, A. Ourmazd, and K. F. Lee, "Scaling the Si MOSFET: From bulk to SOI to bulk," *IEEE Trans. Electron Devices*, vol. 39, no. 7, pp. 1704–1710, Jul. 1992, doi: 10.1109/16.141237.

[22] J. Kang, W. Liu, D. Sarkar, D. Jena, and K. Banerjee, "Computational study of metal contacts to monolayer transition-metal dichalcogenide semiconductors," *Phys. Rev. X*, vol. 4, no. 3, 2014, Art. no. 031005, doi: 10.1103/PHYSREVX.4.031005.

[23] E. Ber, R. W. Grady, E. Pop, and E. Yalon, "Pinpointing the dominant component of contact resistance to atomically thin semiconductors," 2021, *arXiv:2110.02563*.

[24] A. Prakash, H. Ilatikhameneh, P. Wu, and J. Appenzeller, "Understanding contact gating in Schottky barrier transistors from 2D channels," *Sci. Rep.*, vol. 7, no. 1, pp. 1–9, Oct. 2017, doi: 10.1038/s41598-017-12816-3.

[25] D. S. Schulman, A. J. Arnold, and S. Das, "Contact engineering for 2D materials and devices," *Chem. Soc. Rev.*, vol. 47, no. 9, pp. 3037–3058, May 2018, doi: 10.1039/c7cs00828g.

[26] K. Sotthewes et al., "Universal Fermi-level pinning in transition-metal dichalcogenides," *J. Phys. Chem. C*, vol. 123, no. 9, pp. 5411–5420, Feb. 2019, doi: 10.1021/acs.jpcc.8b10971.

[27] F. Giannazzo, E. Schilirò, G. Greco, and F. Roccaforte, "Conductive atomic force microscopy of semiconducting transition metal dichalcogenides and heterostructures," *Nanomaterials*, vol. 10, no. 4, p. 803, Apr. 2020, doi: 10.3390/nano10040803.

[28] K. K. H. Smithe, S. V. Suryavanshi, M. M. Rojo, A. D. Tedjarati, and E. Pop, "Low variability in synthetic monolayer MoS_2 devices," *ACS Nano*, vol. 11, no. 8, pp. 8456–8463, Jul. 2017, doi: 10.1021/acsnano.7b04100.

[29] A. C. Domask, K. A. Cooley, B. Kabius, M. Abraham, and S. E. Mohney, "Room temperature van der Waals epitaxy of metal thin films on molybdenum disulfide," *Cryst. Growth Des.*, vol. 18, p. 44, Apr. 2018, doi: 10.1021/acs.cgd.8b00257.

[30] T. N. Walter, K. A. Cooley, A. C. Domask, and S. E. Mohney, "Nickel diffusion into MoS_2 and the effect of annealing on contact resistance," *Mater. Sci. Semicond. Process.*, vol. 107, Mar. 2020, Art. no. 104850, doi: 10.1016/J.MSSP.2019.104850.

[31] K. Schauble et al., "Uncovering the effects of metal contacts on monolayer MoS_2," *ACS Nano*, vol. 14, no. 11, pp. 14798–14808, Nov. 2020, doi: 10.1021/acsnano.0c03515.

[32] C. English, G. Shine, V. Dorgan, K. Saraswat, and E. Pop, "Improved contacts to MoS_2 transistors by ultra-high vacuum metal deposition," *Nano Lett.*, vol. 16, pp. 3824–3830, May 2016, doi: 10.1021/acs.nanolett.6b01309.

[33] G. Mirabelli, P. K. Hurley, and R. Duffy, "Physics-based modelling of MoS_2: The layered structure concept," *Semicond. Sci. Technol.*, vol. 34, no. 5, Apr. 2019, Art. no. 055015, doi: 10.1088/1361-6641/AB121B.

[34] G. Arutchelvan et al., "From the metal to the channel: A study of carrier injection through the metal/2D MoS_2 interface," *Nanoscale*, vol. 9, no. 30, pp. 10869–10879, 2017, doi: 10.1039/c7nr02487h.

[35] A. J. Arnold, D. S. Schulman, and S. Das, "Thickness trends of electron and hole conduction and contact carrier injection in surface charge transfer doped 2D field effect transistors," *ACS Nano*, vol. 14, no. 10, pp. 13557–13568, Oct. 2020, doi: 10.1021/ACSNANO.0C05572.

[36] (2022). *IEEE International Roadmap for Devices and Systems IEEE IRDS*. [Online]. Available:https://irds.ieee.org/

[37] D. Somvanshi, E. Ber, C. S. Bailey, E. Pop, and E. Yalon, "Improved current density and contact resistance in bilayer $MoSe_2$ field effect transistors by AlO_x capping," *ACS Appl. Mater. Interface*, vol. 12, no. 32, pp. 36355–36361, Aug. 2020, doi: 10.1021/acsami.0c09541.

[38] A.-S. Chou et al., "High on-current 2D nFET of 390 μA/μm at V_{DS} = 1 V using monolayer CVD MoS_2 without intentional doping," in *Proc. IEEE Symp. VLSI Technol.*, Jun. 2020, pp. 1–2.